1 # Streamflow indices to identify catchment drivers of
2 # hydrograph

3 Jeenu Mathai[1] and Pradeep P. Mujumdar[1,2]

4 [1]Department of Civil Engineering, Indian Institute of Science, Bangalore, India

5 [2]Interdisciplinary Centre for Water Research, Indian Institute of Science, Bangalore, India

6 *Correspondence to*: P. P. Mujumdar (pradeep@iisc.ac.in)

8 **Abstract.** Streamflow indices are flow descriptors that quantify the streamflow dynamics, which are usually

9 determined for a specific basin and are distinct from other basin features. The flow descriptors are appropriate for

10 large-scale and comparative hydrology studies, independent of statistical assumptions and can distinguish signals

11 that indicate basin behavior over time. In this paper, the characteristic features of the hydrograph's temporal

12 asymmetry due to its different underlying hydrologic processes are primarily highlighted. Streamflow indices

13 linked to each limb of the hydrograph within the time-irreversibility paradigm are distinguished with respect to

14 its processes driving the rising and falling limbs. Various streamflow indices relating the rising and falling limbs,

15 and the catchment attributes such as climate, topography, vegetation, geology and soil are then correlated. Finally,

16 the key attributes governing rising and falling limbs are identified. The novelty of the work is on differentiating

17 hydrographs by their time irreversibility property and offering an alternative way to recognize primary drivers of

18 streamflow hydrographs. A set of streamflow indices at the catchment scale for 671 basins in the Contiguous

19 United States (CONUS) is presented here. These streamflow indices complement the catchment attributes

20 provided earlier (Addor et al., 2017) for the CAMELS data set. A series of spatial maps describing the streamflow

21 indices and their regional variability over the CONUS is illustrated in this study.

23 ## 1 Introduction

24 Hydrologists use data to underpin the hydrologic system by identifying several unique catchment signatures and

25 employ various flow descriptors independent of statistical assumptions yet capable of capturing signals that reflect

26 the basin's long-term unique behavior. Hydrological indices, commonly referred to as hydrologic metrics,

27 hydrologic signatures, or diagnostic signatures, are quantitative flow metrics that characterize statistical or

28 dynamical hydrological data series (McMillan, 2021). Specifically, streamflow indices are flow descriptors

29 derived from discharge time-series data, and a considerable collection of indices are available to aid in the better

30 characterization of hydrological features, ranging from basic statistics like the mean to more sophisticated metrics

31 (Addor et al., 2018; McMillan, 2021). In many cases, daily streamflow records are not permitted for redistribution;

32 however, researchers have computed streamflow indices and made them publicly accessible.

33

34 Hydrological indices are increasingly used in emerging areas such as global-scale hydrologic modeling and large-

35 sample hydrology to extract relevant information and compare the different watershed processes (Addor et al.,

36 2017, 2018; McMillan, 2021). These indices offer an indirect way to explore hydrological processes as well as

37 provide insights into hydrologic behavior in catchments where data other than streamflow is restricted and are

38 widely used in process exploration, model calibration, model selection, and catchment classification (Addor et al.,

39 2018; Clark et al., 2011; Kuentz et al., 2017; McMillan et al., 2011; Sawicz et al., 2011). McMillan (2021)

40 presented a classification that differentiates between statistics- and dynamics-based signatures and between

41 signatures at different timescales.

42

43 The relevance of time irreversibility (or temporal asymmetry) of streamflow variability on a daily scale has been

44 emphasized in recent studies (Koutsoyiannis, 2020; Mathai and Mujumdar, 2019; Serinaldi and Kilsby, 2016) the

45 disparity in physical mechanisms driving the hydrograph's ascension and recession limbs (Fig.1) contributes to

46 time irreversibility. Unlike other variables such as temperature, wind, precipitation, time irreversibility has been

47 marked for streamflow at a daily scale (Koutsoyiannis, 2020). Moreover, the various segments of the recession

48 phase represent different phases in the flow process. As a result, time irreversibility must be acknowledged in

49 streamflow analysis, accounting for the distinction of the recession into different segments, with a faster recession

50 induced by high discharges caused by surface runoff and a slower recession caused by baseflow (Fig.1), and the

51 characterization of the recession rates separately (Mathai and Mujumdar, 2019). In this study, streamflow indices

52 are chosen to better understand different hydrological processes by recognizing the streamflow hydrograph's

53 temporal asymmetry.

54
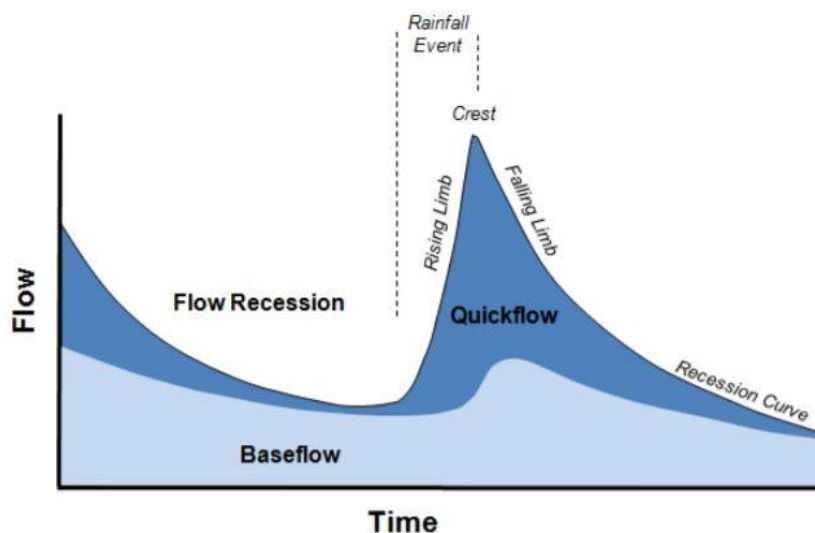
55
56 **Figure 1.** Schematic representation of rising limb and falling limb
57 (source: Environment Southland;
58 https://www.es.govt.nz/environment/water/groundwater/groundwater-monitoring)

59

60 **2 Methods**

61 To facilitate a comprehension of various hydrological processes and streamflow hydrograph drivers, the study

62 employs streamflow indices considering the streamflow hydrograph's temporal asymmetry. The description of

63 indices used in this study are tabulated in Table 1. Streamflow indices linked to each limb of the streamflow

64 hydrograph within the time-irreversibility paradigm are distinguished since hydrographs have rising and falling

limbs. The following indices are considered in the rising limb category: 1) rising limb density, 2) rising limb shape parameter, and 3) rising limb scale parameter. In contrast, 1) falling limb density 2) slope of upper recession (upper recession coefficient) 3) slope of lower recession (lower recession coefficient) are selected in falling limb category. The next step is to compute these indices for a large number of catchments and correlate them with attributes such as climate, topography, vegetation, geology, and soil. The streamflow indices can be correlated explicitly since sub-categories are involved in each of the catchment attributes discussed above. Finally, the key attributes governing ascension and recession limbs can be summarized and identified. This work's main novelty is to differentiate hydrographs by their time irreversibility property and using their associated indices by offering an alternative way to recognize primary drivers of streamflow hydrographs. The specifics of indices are explained further below.

Rising limb density (RLD) is defined as the ratio of the number of rising limbs and the cumulative time of rising limbs (Shamir et al., 2005). RLD is a hydrograph shape descriptor without considering the flow magnitude (Fig. 2) and the expression for RLD is given as,

$$RLD = \frac{N_{RL}}{T_R} \tag{1}$$

The ratio of the number of falling limbs to the cumulative time of falling limbs is termed as falling limb density (FLD) (Fig. 2) (Shamir et al., 2005). The expression for FLD is given as,

$$FLD = \frac{N_{FL}}{T_F} \tag{2}$$

Table 1. Hydrological descriptors with temporal asymmetry.

Sl.no	Attribute	Description	Unit	Data source	References
1	RLD	Rising limb density	day^{-1}	N15 – USGS data	Shamir et al. (2005)
2	FLD	Falling limb density	day^{-1}		
3	a	ascension limb scale parameter	-		Mathai and Mujumdar, (2019)
4	b	ascension limb shape parameter	-		
5	b_1	Upper recession coefficient	-		
6	b_2	Lower recession coefficient	-		
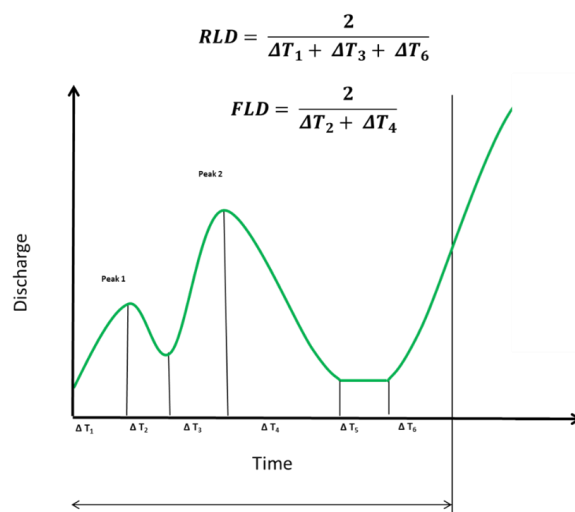
Figure 2. Schematic example of rising limb density (RLD) and falling limb density (FLD) calculation (Shamir et al., 2005).

The diurnal increments of streamflow are fitted with an appropriate probability density function to depict the shape of the ascension limbs which occur on wet days. The Weibull distribution reflects the diurnal increments of streamflow that occur on wet days reasonably well (Mathai and Mujumdar, 2019; Stagge and Moglen, 2013; Szilagyi et al., 2006), and the scale 'a'' and shape 'b'' parameters of the Weibull distribution are computed for each catchment by using observed diurnal increments of streamflow. In contrast, an exponential recession is used to capture the shape of the recession limbs on dry days of the daily hydrograph, representing the falling limbs' underlying dynamics (Mathai and Mujumdar, 2019). As the upper recession refers to the fast flow following a storm event and the lower recession refers to the baseflow recession, falling limb modeling is done in two stages.

The study uses indices related to ascension limb (viz., RLD, ascension limb scale parameter, ascension limb shape parameter) and recession limb (viz., FLD, upper recession coefficient, lower recession coefficient) to summarize the characteristic shape of steeper rising and gradually declining falling limb and its application in understanding the role of various drivers of catchment attributes in streamflow generation.

3 Contributions of the Study

The analysis employs a collection of indices drawn from hydrograph shape diagnoses, which extracts information about a basin's ascension and recession limbs' inherent properties. The principle of time irreversibility is encapsulated by six streamflow indices that describe and characterize a streamflow hydrograph's shape, and indices for a particular basin are consistent and distinct from indices from other basins.

105   The goals of this study are as follows: i) to identify the key drivers of streamflow hydrographs (in terms
106   of catchment attributes) using time-irreversibility-based indices ii) to present a spatial map-based attribute
107   class of time-irreversibility-based indices for a large sample hydrology dataset.

108   As shown in numerous ways/studies in the literature, our notion of time-irreversibility and its indices
109   could also do a reasonable job of articulating the catchment drivers of streamflow hydrographs. This
110   study presents an attribute class of hydrograph shape descriptors with temporal asymmetry. The
111   significance of large sample hydrology datasets in open hydrologic science and their potential to improve
112   hydrological studies' transparency is also underlined in this study.

113   **4 Motivation to extend to large sample hydrology**

114   Large-sample hydrology (LSH) gathers information from a larger number of catchments to gain a more
115   comprehensive understanding of hydrological processes and to go beyond individual case studies. LSH
116   helps identify catchment behavior and leads one to derive precise conclusions regarding different
117   hydrological processes and models (Addor et al., 2020). Studies involving large sample catchments help
118   in understanding the drivers of hydrological change (Blöschl et al., 2019), in assessing hydrological
119   similarity and classification (Berghuijs et al., 2014; K. A. Sawicz et al., 2014), in predictions in ungauged
120   basins (Ehret et al., 2014), and in analysing model and data uncertainty (G. Coxon et al., 2014) and foster
121   hydrology research by standardizing and automating the creation of large sample hydrology datasets
122   worldwide (Addor et al., 2020). LSH assists in exploring interrelationships between numerous catchment
123   attributes related to landscape, climate, and hydrology (Addor et al., 2017; Alvarez-Garreton et al., 2018;
124   Gupta et al., 2014; Newman et al., 2015; K. Sawicz et al., 2011) and generalizing rules that can
125   significantly improve the predictability of the water cycle (Alvarez-Garreton et al., 2018).

126   The primary challenges in fostering LSH are data availability and accessibility, which seriously hinder
127   its use in data-scarce regions. Despite the fact that a few large-scale hydrology studies have been
128   undertaken, the number of publicly available large-scale datasets is still restricted (Addor et al., 2017,
129   2020; Coxon et al., 2020). Moreover, licensing restrictions and strict access policies make the datasets
130   rarely available to the public (Coxon et al., 2020).

131   Model Parameter Estimation Experiment project (MOPEX) dataset (Duan et al., 2006), Canadian model
132   parameter experiment (CANOPEX) database (Arsenault et al., 2016), Global Streamflow Indices and
133   Metadata Archive (Do et al., 2018; Gudmundsson et al., 2018), Global Runoff Reconstruction (Ghiggi et
134   al., 2019), HydroATLAS (Linke et al., 2019) and the Catchment Attributes and MEteorology for Large-
135   Sample studies (CAMELS) (Addor et al., 2017) are notable contributions of open and accessible large
136   sample catchment datasets (Coxon et al., 2020).

137   Addor et al. (2017) introduced a new dataset (CAMELS) made publicly available for large-sample
138   hydrological studies. This dataset covers meteorological and streamflow datasets provided by Newman
139   et al. (2015) and provides quantitative metrics for a large variety of attributes for 671 catchments in the
140   contiguous United States (CONUS). Streamflow records are available in the dataset from 1990 to 2009
141   for the 671 catchments, which are minimally influenced by human activities (Addor et al., 2017).

142 The CAMELS dataset prompted hydrological research by enabling open access to hydrologic data and
143 establishing a common standard across the database. CAMELS promoted open access to datasets for the
144 United States, and it is eventually expanded to the United Kingdom (CAMELS-GB), Chile (CAMELS-
145 CL), and Brazil (CAMELS-BR). The CAMELS proposes five classes of catchment attributes, namely
146 location, topography, geology, land cover characteristics, climatic indices, and hydrological signatures,
147 in order to promote common standards and formats in large sample studies (Addor et al., 2017). The
148 concept of time irreversibility-based streamflow indices is then applied to CAMELS catchments with the
149 goal of encouraging large sample hydrology studies.

150 **5 Dataset used**

151 Section 5 provides the description of the dataset used and the study area chosen. This study employs the
152 CAMELS dataset, which encompasses daily discharge data and catchment attributes for 671 catchments
153 (Fig. 3) across the continental United States, representing a diverse set of catchments with long
154 streamflow time series covering a wide range of hydro-climatic conditions (Addor et al., 2017). The time
155 frame chosen for the analysis is from 1 October 1989 to 30 September 2009 (Addor et al., 2017). The
156 topographic characteristics of CAMELS dataset are represented in Fig. 4. Except for the Appalachian
157 Mountains, the eastern part of the Continental United States is much flatter than the western portion,
158 according to mean elevation and mean slope maps (Fig. 4.a and 4.b). Figure 4.c depicts the spatial pattern
159 of catchment size, highlighting presence of some catchments with an area greater than 10,000 km^2.

160

161

162
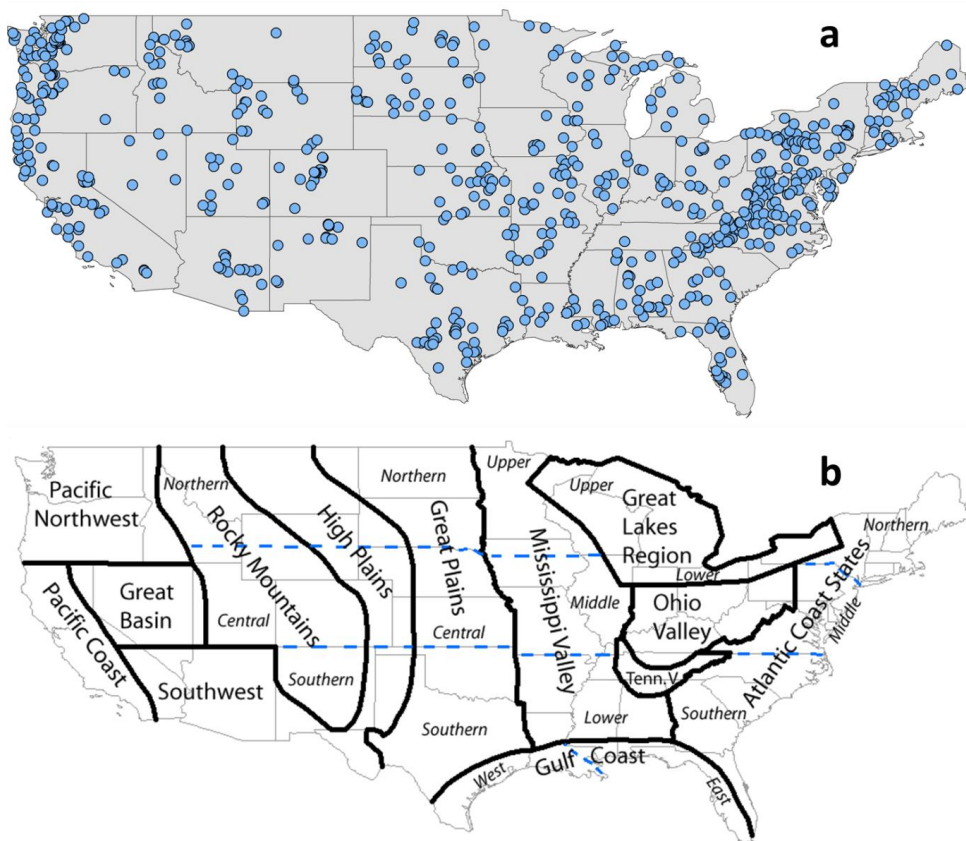
Figure 3. (a) Map of 671 CAMELS catchments in the continental United States considered in this study. (b) Geographical regions of US according to NOAA National Centers for Environmental Information referred for the analysis (source: NOAA National Centers for Environmental Information; https://www.ncdc.noaa.gov/temp-and-precip/drought/nadm/geography).
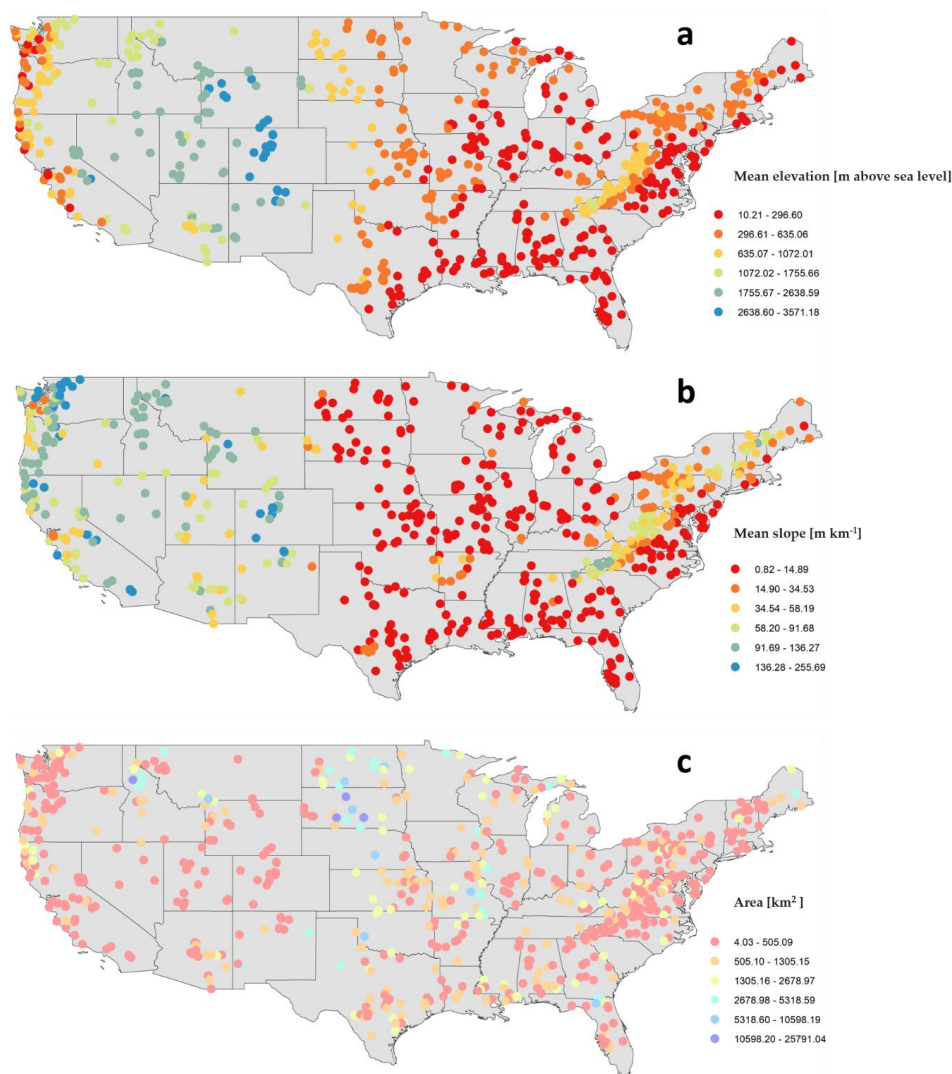
Figure 4. Maps of topographic characteristics of CAMELS catchments over the CONUS (Addor et al., 2017). (a) Mean elevation [m above sea level] (b) Mean slope [m km⁻¹] (c) Area [km²]. The eastern US seems to have a much flatter mean elevation and mean slope than the western US, which significantly influences catchment behavior. The majority of the catchments are noticed to be smaller, with an area of fewer than 3000 km².

179   **5.1 Catchment attributes**

180   The landscape of each catchment is described using multiple attributes, which can be divided into various
181   classes as shown in Table 2 (Addor et al., 2017). The details of the attributes used in this study is
182   summarized in Table 2.

183   **Table 2.** CAMELS attributes (Addor et al., 2017)

184

185

Sl.no	Attribute	Description	Unit
Climatic indices			
1	aridity	aridity (ratio of mean PET to mean precipitation)	-
2	p_seasonality	seasonality and timing of precipitation (positive (negative) values indicate that precipitation peaks in summer (winter); values close to 0 indicate uniform precipitation throughout the year)	-
3	frac_snow	fraction of precipitation falling as snow	-
4	high_prec_freq	frequency of high precipitation days	days yr^{-1}
5	high_prec_dur	average duration of high precipitation events	days
6	low_prec_freq	frequency of dry days	days yr^{-1}
7	low_prec_dur	average duration of dry periods	days
Land cover characteristics			
8	Forest_frac	forest fraction	-
9	Lai_max	maximum monthly mean of the leaf area index	-
10	Gvf_max	maximum monthly mean of the green vegetation fraction	-
Soil characteristics			
11	soil_depth_pelletier	depth to bedrock	m
12	sand_frac	sand fraction	%
13	clay_frac	clay fraction	%
Geological characteristics			
14	geol_porosity	subsurface porosity	-
15	geol_permeability	subsurface permeability (log10)	m^2

186
187
188
189
190
191
192
193
194
195

6 Results and Discussion

The first sub-section below looks at the regional variability of the streamflow indices used in this study. For the 671 CAMELS catchments, rising limb density, falling limb density, ascension limb scale parameter, ascension limb shape parameter, upper recession coefficient, and lower recession coefficient are computed and given as spatial maps. Streamflow indices are then presented in hydrological clusters to incorporate a more explicit spatial representation of catchment behavior across the CONUS. Catchment attributes cover a broad range of aspects of catchment hydrology such as, land cover, soil, climate, geology, topography and the association between these attributes and streamflow indices is discussed further in the subsequent section. As the climate is the most important factor in the US for the hydrological behavior for the CAMELS dataset (Jehn et al., 2020), the influence of climatic factors on streamflow indices is finally studied.

6.1 Spatial Variability in Streamflow Indices

Streamflow indices related to rising limbs and falling limbs are computed for the selected catchments and displayed in spatial maps as shown in Fig. 5 and Fig. 6, respectively. The spatial analysis is based on the United States' geographical areas (for details, refer to Fig. 3b) as defined by NOAA's National Centers for Environmental Information and is referred to in the following spatial maps. Furthermore, ten clusters provided by Jehn et al. (2020) to represent the discrete hydrological behaviors of the continental United States are adopted in this study to understand the regional variability of catchment behavior. Figure S1 and Table S1 present the location map and details of the ten clusters.

In terms of geographical regions, the rising limb density is highest over the Atlantic coast states, Ohio valley, Lower Mississippi Valley, Southern Great Plains, Southwest and Pacific, and lowest along the Upper Great Lakes region, Upper Mississippi Valley, Great Basin, and Northern Rocky Mountains, Northern Interior Plains, and East of Gulf Coast (Fig. 5.a). Further, in terms of hydrological clusters, Appalachian Mountains (Cluster 10), Southeastern and Central Plains (Cluster 1) and all Southern most states of the US (Cluster 9) witness high rising limb densities and these clusters are characterized by a high forest fraction, low aridity, and high frequency of high precipitation events, respectively (Fig. 6.a). Northwestern Forested Mountains (Clusters 3, 4), located in the mountains of the western US, experience low values of rising limb density as these clusters are characterized by a dominant summer peak of discharge caused by rapid snowmelt (Fig. 6.a).

Considerably low values of rising limb scale parameters are experienced over the Rocky Mountains, High Plains, Great Plains, Upper Mississippi Valley, Great Basin, Southwest, and the Great Lakes regions, whereas the Pacific Northwest shows high values of rising limb scale parameters (Fig. 5.b). Clusters (5, 7) over the Northwestern Forested Mountains of CONUS experience very high values of rising limb scale parameters (Fig. 6.b). These catchments have the highest discharge, especially in the early summer, due to a combination of high precipitation and snowmelt. Further, the region in the Continental US which receives the highest precipitation is included in Cluster 5. Moreover, Cluster 5 consists of a large proportion of forest. Again, Cluster 7 with high values of rising limb scale parameter is characterized by high fraction of precipitation falling as snow. Low values of rising limb scale parameters are shown by Clusters 2, 8, 9. This is because of low water availability, low snow fraction precipitation falling as snow, and high evaporation experienced in these regions.

233   Low rising limb shape parameter occurs along the Great Plains, Mississippi Valley, Pacific coast, and the west of
234   Gulf Coast (Fig. 5.c). In contrast, the shape parameter over the Rocky Mountains, High Plains, Great Basin, Pacific
235   Northwest, and the Great Lakes region witnesses the highest values of rising limb shape parameters (Fig. 5.c). All
236   the catchments located in the Southern states of the US (Cluster 9), Great Plains and North American deserts
237   (Cluster 8), and the Central Plains (Cluster 2) characterize low values of rising limb shape parameters (Fig. 6.c).
238   This is due to low water availability, low snow fraction precipitation falling as snow, low leaf area index, and high
239   evaporation experienced in these regions. High values of rising limb shape parameters are seen in Clusters 3, 4
240   (Fig. 6.c) located in the Northwestern Forested Mountains of the western US, dominant with a summer peak of
241   discharge caused by rapid snowmelt.

242   Catchments with a high falling limb density are predominantly located along the Great Basin and the Rocky
243   Mountains and in the High Plains region (Fig. 7.a). Clusters 4, 2, 8 over Northwestern Forested Mountains, Central
244   Plains, Great Plains, and North American deserts characterize higher magnitudes of falling limb density, and
245   Clusters 6, 7 over Marine West Coast Forests and Western Cordillera smaller falling limb densities (Fig. 8.a).
246   This is due to less presence of forest cover in these arid regions.

247   Similarities exist between the patterns of the upper recession coefficient and the lower recession coefficient (Fig.
248   7.b and Fig. 7.c). Clusters 3, 4 located in the Northwestern Forested Mountains, which have overall low discharge,
249   show low values of upper and lower recession coefficients (Fig. 8.b and Fig. 8.c). Clusters 2, 9, located in the
250   eastern US, witness high values of recession coefficients; due to low slope inclinations, water takes a long time
251   to reach the outlet (Fig. 8.b and Fig. 8.c).

252
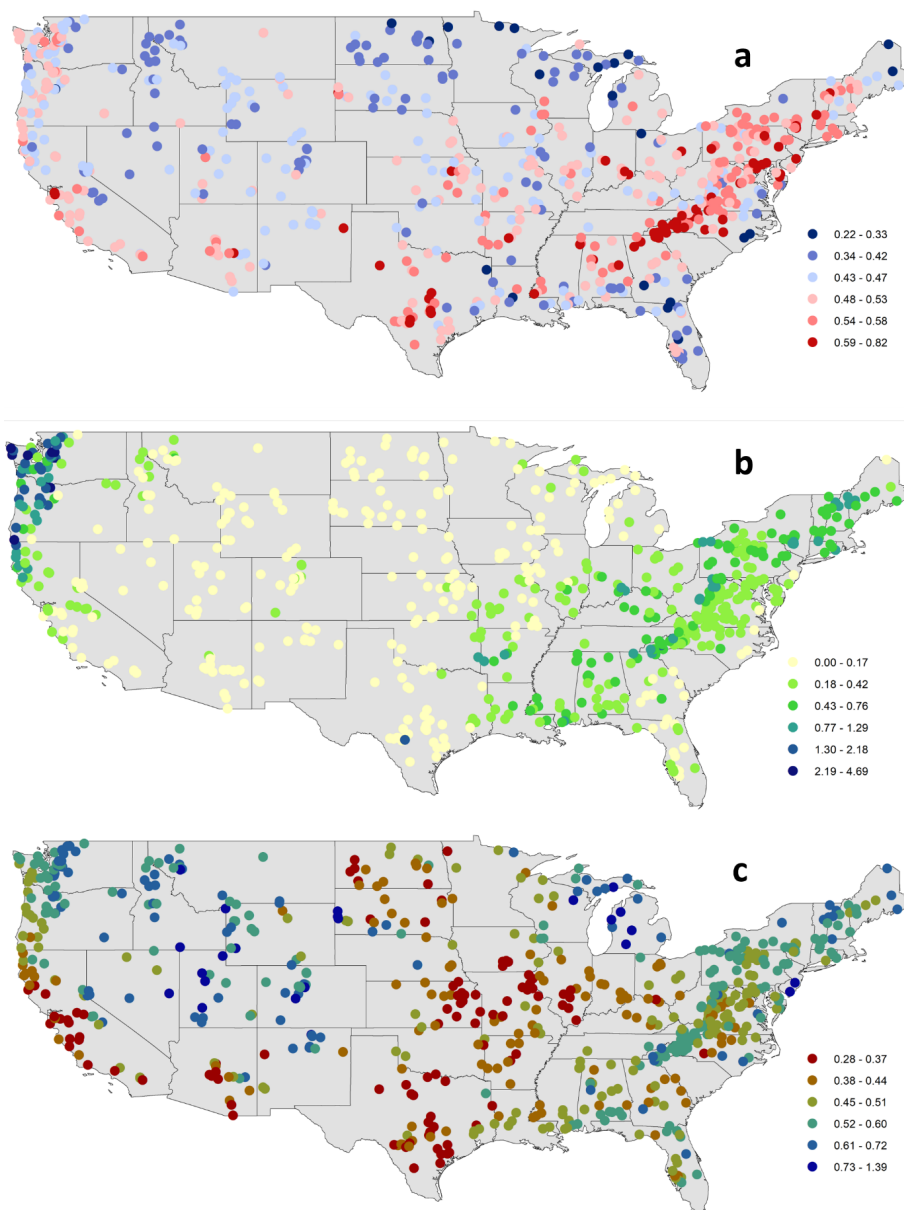
Figure 5. Spatial maps of streamflow indices associated with a rising limb (a) rising limb density [day^{-1}], (b) rising limb scale parameter, (c) rising limb shape parameter over the CONUS**.** The Atlantic coast states, Ohio Valley, Lower Mississippi Valley, Southern Great Plains, Southwest, and Pacific have the highest rising limb density, while the Upper Great Lakes region, Upper Mississippi Valley, Great Basin, Northern Rocky Mountains, Northern Interior Plains, and East of Gulf Coast have the lowest. The Rocky Mountains, High Plains, Great Plains, Upper Mississippi Valley, Great Basin, Southwest, and Great Lakes regions have low values of rising limb scale parameters, but the Pacific Northwest has high values of rising limb scale parameters. The Great Plains, Mississippi Valley, Pacific coast, and west of Gulf Coast have low rising limb shape parameters. The shape parameter has the greatest values of rising limb shape parameters over the Rocky Mountains, High Plains, Great Basin, Pacific Northwest, and Great Lakes regions.

263

264
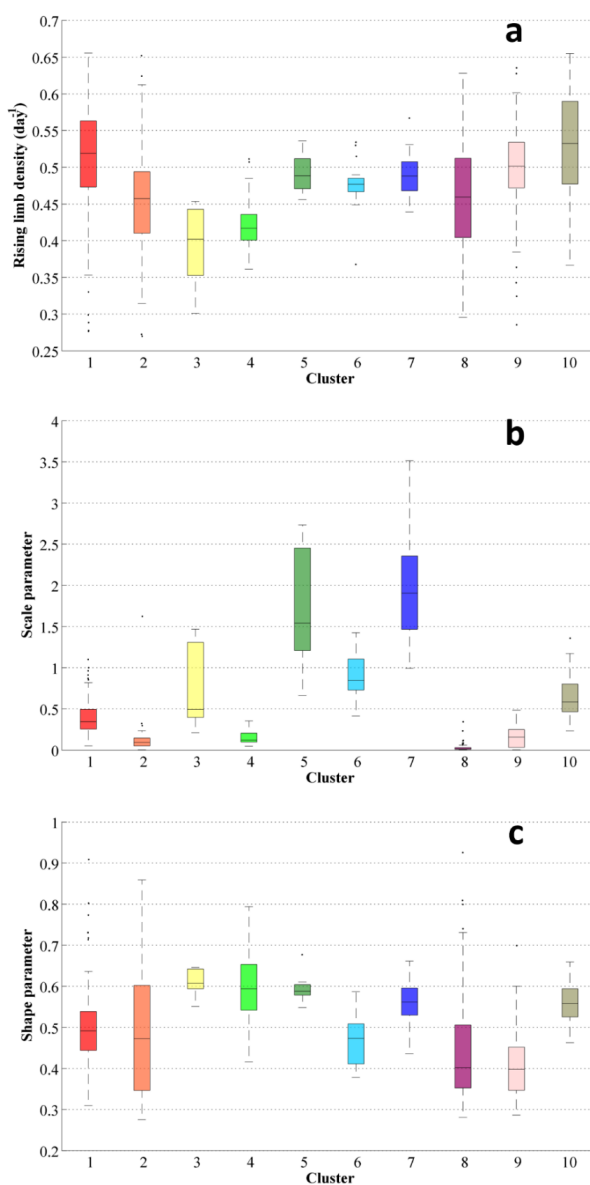
Figure 6. Boxplots of the hydrological descriptors linked with the rising limb (a) rising limb density [day⁻¹], (b) rising limb scale parameter, (c) rising limb shape parameter of the clusters over the CONUS. High rising limb densities are observed in Clusters 10, 1, and 9, which are characterized by a high forest fraction, low aridity, and a high frequency of high precipitation events, respectively. Rising limb scale parameters are exceptionally high in Clusters 5, 7. Due to a combination of high precipitation and snowmelt, these catchments have the highest discharge. Because of the low water availability, low snow fraction precipitation falling as snow, low leaf area index, and high evaporation experienced in these areas, catchments in Cluster 9, Cluster 8, and Cluster 2 have low values of rising limb shape parameters.

273

274
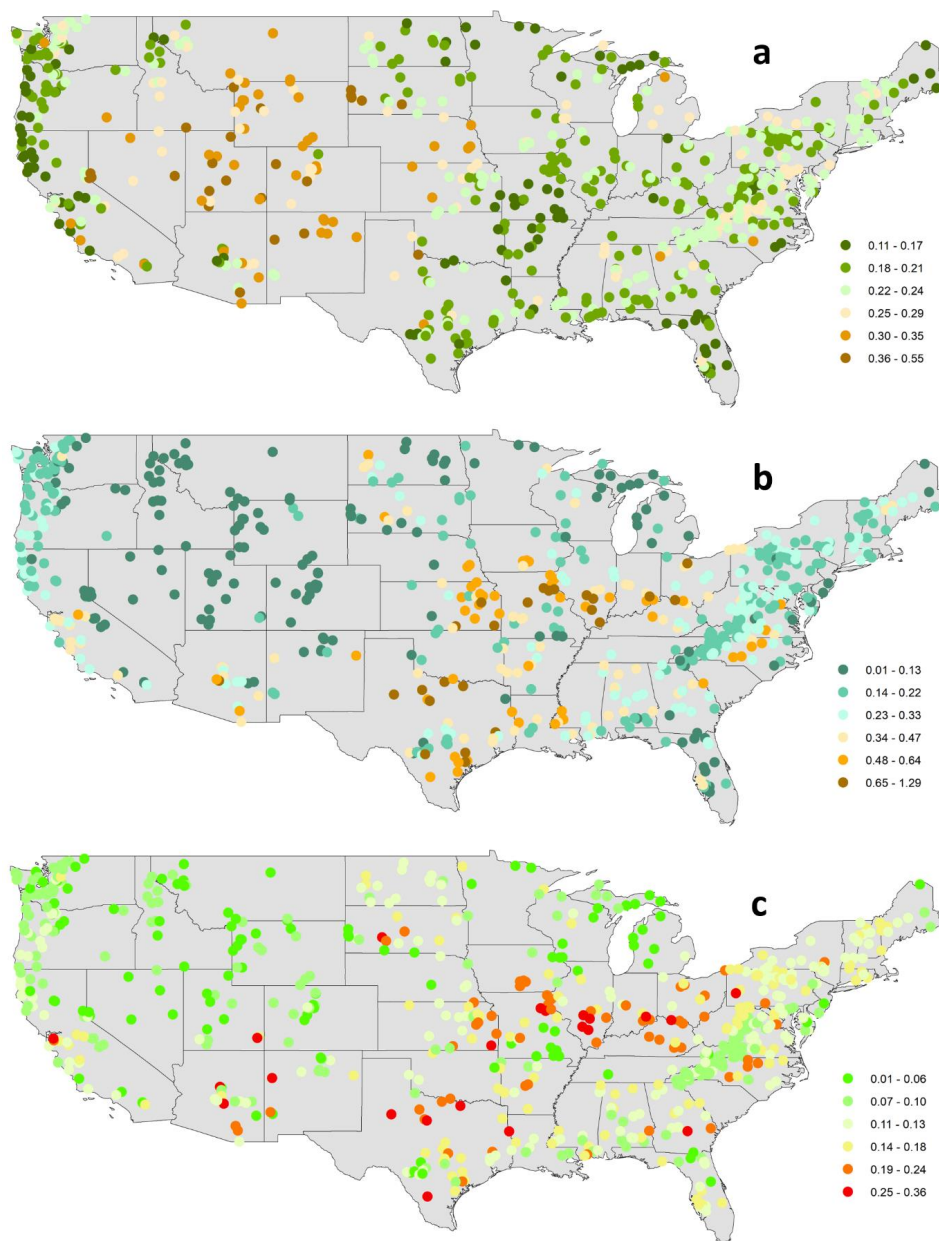
Figure 7. Regional variability of streamflow indices associated with the falling limb (a) falling limb density
[day^{-1}], (b) upper recession coefficient, (c) lower recession coefficient over the CONUS. The Great Basin and the
Rocky Mountains, and the High Plains region have high falling limb density. The patterns of the upper recession
coefficient and the lower recession coefficient are similar.

279
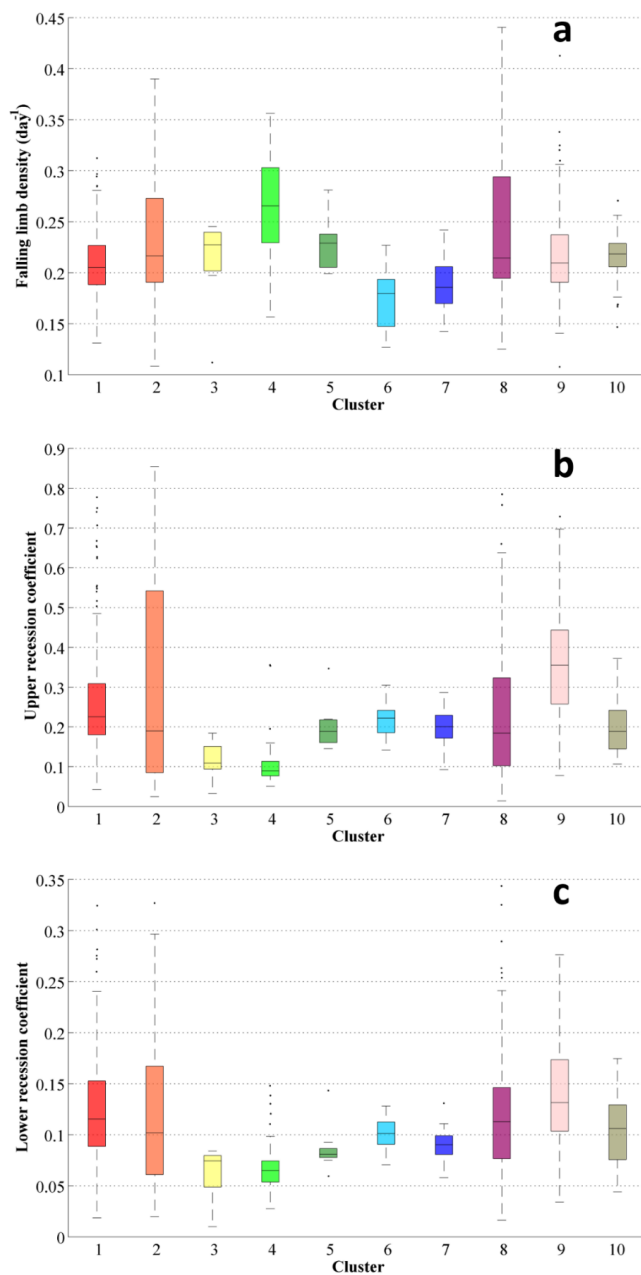
Figure 8. Boxplots of the streamflow indices related with the falling limb (a) falling limb density [day^{-1}], (b) upper recession coefficient, (c) lower recession coefficient of the clusters. Clusters 4, 2, 8 have higher falling limb densities, while Clusters 6, 7 have lower falling limb densities due to the less forest cover in these arid areas. Clusters 3, 4, which have a low discharge, have low upper and lower recession coefficients. Clusters 2, 9 have high recession coefficients due to low slope inclinations.

286

6.2 Relation of the Flow Descriptors and the Catchment Attributes

288 The association between the flow descriptors related to rising and falling limbs and catchment attributes is
289 examined in this section. Table 3 shows the relation of streamflow indices linked with rising limb, and Table 4
290 shows the association of indices of the falling limb with catchment attributes. Across all five attribute classes, the
291 vegetation/land cover attributes positively correlate with all rising limb indices (Table 3). It can be seen that the
292 rising limb density shows a positive correlation with all the three vegetation density indicators, namely fraction
293 of forest, maximum leaf area index, maximum green vegetation fraction (Table 3).

294

295 However, it is observed that the rising limb scale parameter shows a negative correlation with climate and a
296 positive association with the vegetation attributes (Table 3). Aridity and frequency of precipitation (Table 3)
297 display a strong negative association with the rising limb scale parameter. It is noted that the rising limb shape
298 parameter indicates a positive correlation with vegetation attributes and the fraction of precipitation falling as
299 snow, mean slope, mean elevation, and sand fraction whereas, it negatively correlates with precipitation
300 frequency.

301

302 Falling limb density is mainly governed by climate indices and is negatively correlated with the land cover
303 characteristics (Table 4). Mean elevation also strongly characterizes the nature of the falling limb density. Besides,
304 aridity and fraction of precipitation falling as snow are also positively correlated with falling limb density.
305 Recession coefficients are negatively correlated with topographic indices (Table 4). Further, the recession
306 coefficients show a positive correlation with clay and negative correlations with the fraction of precipitation falling
307 as snow, forest fraction, and sand fraction. Moreover, the geology attributes such as subsurface porosity reveal a
308 positive correlation to recession coefficients and a negative with subsurface permeability (Table 4).

309

310

311

312 **Table 3.** Correlation between streamflow indices linked with rising limb and the catchment attributes. Green
313 colored coefficients represent positive correlation, and the red-colored correlation coefficients represent the
314 negative correlation. The vegetation/land cover attributes positively correlate with all rising limb indices amongst
315 all five attribute groups. It can be seen that the rising limb density has a positive relationship with all three
316 vegetation density measures. The rising limb scale parameter, has a negative association with climate and a
317 positive relationship with vegetation attributes. The rising limb shape parameter positively correlates with
318 vegetation attributes and the fraction of precipitation that falls as snow, mean slope, mean elevation, and sand
319 fraction.

Spearman rank correlation coefficients	Topography			Climate							Soil			Land cover			Geology	
	Area	Mean elevation	Mean slope	Precipitation seasonality	Frac of precp as snow	Aridity	High precp freq	High precp dur	Low precp freq	Low precp dur	Depth to bedrock	Sand frac	Clay frac	Forest frac	LAI maximum	Green veg frac max	Subsurface porosity	Subsurface permeability
Rising limb density	-0.30	-0.20			-0.33	-0.10	0.08	-0.15			-0.32	-0.28	0.26	0.10	0.20	0.18	-0.16	-0.11
Scale parameter	-0.17	-0.13	0.35	-0.36		-0.53	-0.56		-0.63	-0.25	-0.21		-0.15	0.46	0.41	0.44		
Shape parameter		0.41	0.36	-0.14	0.53	-0.16	-0.42		-0.45	-0.29	-0.16	0.37	-0.47	0.41	0.17	0.15	-0.16	

320

321

322

323

324

325

326

327

328

329

330

Table 4. Correlation between streamflow indices linked with falling limb and the catchment attributes. Green colored coefficients represent positive correlation, and the red-colored correlation coefficients represent the negative correlation. Climate factors are the principal drivers of falling limb density and are negatively associated with land cover characteristics. Topographic indicators are negatively correlated with recession coefficients. Furthermore, the recession coefficients reveal a positive association with clay and negative correlations with the fraction of precipitation falling as snow, forest fraction, and sand fraction.

Spearman rank correlation coefficients	Topography			Climate							Soil			Land cover			Geology	
	Area	Mean elevation	Mean slope	Precipitation seasonality	Frac of precp as snow	Aridity	High precp freq	High precp dur	Low precp freq	Low precp dur	Depth to bedrock	Sand frac	Clay frac	Forest frac	LAI maximum	Green veg frac max	Subsurface porosity	Subsurface permeability
Falling limb density	-0.13	0.55	0.18		0.42	0.39	0.12	0.12	0.17	0.11	-0.19			-0.17	-0.37	-0.40	-0.08	
Upper recession coefficient		-0.40	-0.38	0.17	-0.46		0.31	-0.11	0.26		0.19	-0.38	0.52	-0.31	-0.09		0.13	-0.09
Lower recession coefficient		-0.35	-0.37	0.22	-0.39		0.27	-0.17	0.19		0.21	-0.23	0.32	-0.28			0.16	-0.18

339
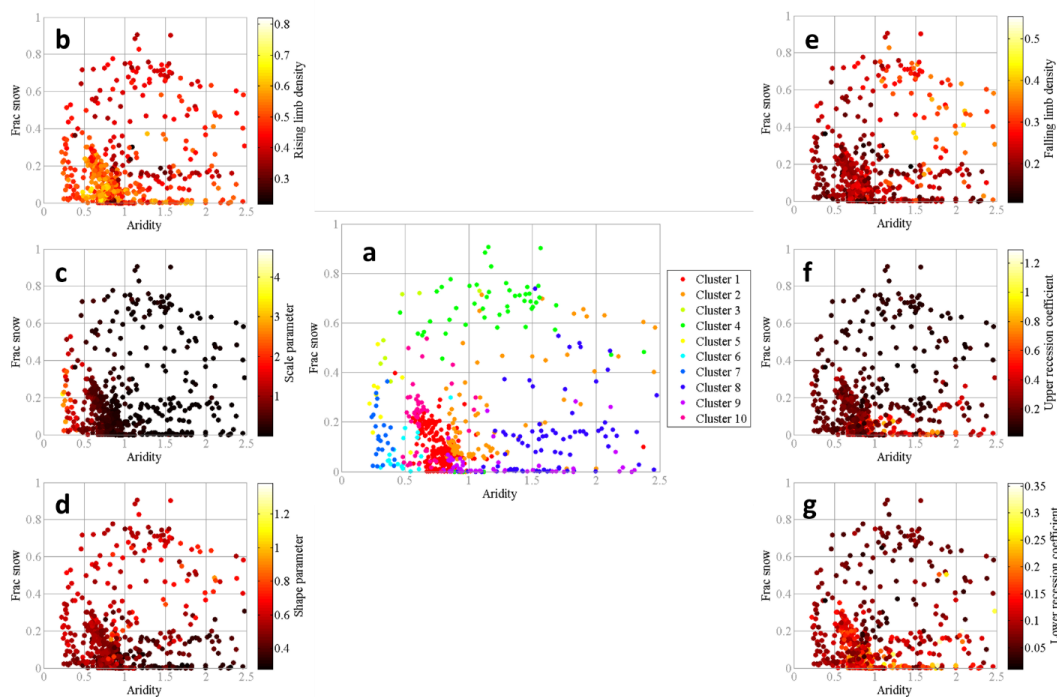
Figure 9. (a) Comparison of the hydrological clusters of Jehn et al. (2020) with the climate index space (fraction of precipitation falling as snow vs. aridity). Single dots show the catchments and are colored by their hydrological clusters. Comparison of the streamflow indices in climate index space (b) rising limb density (c) rising limb scale parameter, (d) rising limb shape parameter, (e) falling limb density, (f) upper recession coefficient, (g) lower recession coefficient for all catchments. Single dots show the catchments and are colored according to the value of the streamflow indices. Low values of rising limb density, high values of the rising limb shape parameter, and low values of recession coefficients are seen in catchments with a humid environment and a high fraction of precipitation falling as snow. In arid climates with a low fraction of precipitation falling as snow, the lowest values of rising limb scale and shape parameters, as well as the highest values of falling limb density, can be seen.

349

350   **6.3 Streamflow Indices with Attributes of Climate**

351   Climate attributes seem to be the most important indicator for hydrological behavior in the United States among

352   the various attribute categories (Jehn et al., 2020). Hence, the flow descriptors are then examined in the climate

353   index space (aridity along x-axis and fraction of precipitation falling as snow along the y-axis) to evaluate the

354   main drivers of the catchments. Single dots show the catchments and are colored by their hydrological clusters

355   (Fig. 9.a).

356   Clusters 5, 6, 7, 1, 10 are characterized by a low fraction of precipitation falling as snow and humid climate,

357   whereas Clusters 3, 4 have humid climate experiencing a high fraction of precipitation falling as snow (Fig. 9.a).

358   Clusters 2, 8, 9 are featured by a low fraction of precipitation falling as snow and arid climate (Fig. 9.a). The three

359   categories mentioned above are referred to as G1, G2, and G3, respectively.

360   Clusters G1 with a low fraction of precipitation falling as snow with humid climate show (Clusters 1, 9, 10) high
361   rising limb densities (Fig. 9.b) and (Clusters 5, 7) high rising limb scale parameters (Fig. 9.c). This is because the
362   rising limb density negatively correlates with fraction of precipitation falling as snow (Fig. 9.b), whereas the rising
363   limb scale parameter negatively correlates with aridity (Fig. 9.c). Moreover, these Clusters G1 experience a low
364   value of (Clusters 6, 7) falling limb density (Fig. 9.e). This is because the falling limb density positively correlates
365   with the climate indices (Fig. 9.e).

366   As mentioned earlier, Clusters G2 with humid climate and with a high fraction of precipitation falling as snow
367   (Clusters 3, 4) display low values of rising limb density as rising limb density correlates negatively with the
368   fraction of precipitation falling as snow (Fig. 9.b). G2 witnesses higher values of rising limb shape parameter due
369   to its negative correlation with aridity and positive correlation with the fraction of precipitation falling as snow
370   (Fig. 9.d). Furthermore, the Clusters of G2 (Clusters 3, 4) show low values of recession coefficients as they depict
371   a strong negative correlation with the fraction of precipitation falling as snow (Fig. 9.f, g).

372   Low values of rising limb scale and shape parameters are noticed for the Clusters 2, 9, 8 (Clusters G3) with arid
373   climate and low fraction of precipitation falling as snow (Fig. 9.c, d) due to its negative correlation with aridity as
374   stated earlier. Cluster 8 experiences the maximum values of falling limb density (Fig. 9.e) where the region
375   witnesses low fraction of snow and arid catchments, due to its strong positive correlates with the aridity.

376   **7 Concluding remarks**

377   Streamflow hydrograph portrays the time distribution of runoff at the point of measurement by a single curve, and
378   the hydrographs are characterized by their time irreversibility property. In this study, the indices related to this
379   characteristic feature are used to study the catchment drivers of streamflow hydrograph. The streamflow indices
380   associated with the time irreversibility of hydrograph open new opportunities to investigate the interaction
381   between topography, soil, climate, vegetation, geology that drive the hydrological behavior of catchments.
382   Moreover, most of the previously presented hydrologic indices are employed only for time-symmetric processes;
383   the importance of the time irreversibility of streamflow is highlighted in this study. The indices associated with
384   rising and falling limbs are primarily correlated to distinct catchment attributes, establishing a relationship
385   between the indices and catchment attributes such as climate, topography, soil, geology, and vegetation to
386   delineate the controlling drivers in corresponding hydrograph sections. A set of streamflow indices with temporal
387   asymmetry for 671 catchments in the United States is presented in this study. The regional variations among
388   catchments over the United States are compared and discussed using the spatial maps of streamflow indices. Such
389   spatial maps of the streamflow indices supplement the hydrometeorological time series and catchment attributes
390   provided by Addor et al. (2017).

391   The study revealed that the rising limb indices such as rising limb density, rising limb shape parameter and rising
392   limb scale parameter correlate positively with vegetation indices. Falling limb density is primarily controlled by
393   climate indices and is negatively correlated with land cover characteristics; the structure of the falling limb density
394   is also closely influenced by mean elevation. Finally, flow descriptors are studied in the climate index space to
395   isolate the runoff generation's leading drivers. High rising limb densities and rising limb scale parameters are
396   observed in catchments with low precipitation falling as snow and a humid climate. It is observed that the
397   catchments with a humid climate and a high fraction of precipitation falling as snow display low values of rising

398   limb density, high values of the rising limb shape parameter, and low values of recession coefficients. The lowest

399   values of rising limb scale and shape parameters, and the highest values of falling limb density, are seen in

400   catchments of arid climates and a low fraction of precipitation falling as snow.

401   In general, the contribution of this work lies in differentiating hydrographs depending on their time irreversibility

402   property and using the corresponding indices to provide an alternative methodology for identifying the drivers of

403   streamflow hydrographs. In the context of large sample hydrology research, the concept of time-irreversibility

404   and the indices associated with it could also be used to describe the drivers at catchment scale.

405

406   *Data availability.* The CAMELS dataset can be found at https://doi.org/10.5194/hess21-5293-2017 (Addor et al.

407   2017).

408   *Competing interests.* The authors declare that they have no conflict of interest.

409   *Acknowledgements.* We would like to thank all the people who created the CAMELS dataset. The funding

410   received from the Ministry of Earth Sciences (MoES), Government of India, through the project, "Advanced

411   Research in Hydrology and Knowledge Dissemination", Project No.: MOES/PAMC/H&C/41/2013-PC-II, is

412   gratefully acknowledged.

413

414   **References**

415

416   Addor, Newman, A. J., Mizukami, N. and Clark, M. P.: The CAMELS data set: catchment attributes and

417   meteorology for large-sample studies, Hydrol. Earth Syst. Sci., 21(10), 5293–5313, doi:10.5194/hess-21-5293-

418   2017, 2017.

419   Addor, Nearing, G., Prieto, C., Newman, A. J., Le Vine, N. and Clark, M. P.: A Ranking of Hydrological

420   Signatures Based on Their Predictability in Space, Water Resour. Res., 54(11), 8792–8812,

421   doi:10.1029/2018WR022606, 2018.

422   Addor, N., Do, H. X., Alvarez-Garreton, C., Coxon, G., Fowler, K. and Mendoza, P. A.: Large-sample hydrology:

423   recent progress, guidelines for new datasets and grand challenges, Hydrol. Sci. J., 65(5), 712–725,

424   doi:10.1080/02626667.2019.1683182, 2020.

425   Alvarez-Garreton, C., Mendoza, P. A., Pablo Boisier, J., Addor, N., Galleguillos, M., Zambrano-Bigiarini, M.,

426   Lara, A., Puelma, C., Cortes, G., Garreaud, R., McPhee, J. and Ayala, A.: The CAMELS-CL dataset: Catchment

427   attributes and meteorology for large sample studies-Chile dataset, Hydrol. Earth Syst. Sci., 22(11), 5817–5846,

428   doi:10.5194/hess-22-5817-2018, 2018a.

429   Alvarez-Garreton, C., Mendoza, P. A., Boisier, J. P., Addor, N., Galleguillos, M., Zambrano-Bigiarini, M., Lara,

430   A., Puelma, C., Cortes, G., Garreaud, R., McPhee, J. and Ayala, A.: The CAMELS-CL dataset: catchment

431   attributes and meteorology for large sample studies – Chile dataset, Hydrol. Earth Syst. Sci., 22(11), 5817–5846,

432   doi:10.5194/hess-22-5817-2018, 2018b.

433   Arsenault, R., Bazile, R., Ouellet Dallaire, C. and Brissette, F.: CANOPEX: A Canadian hydrometeorological

434   watershed database, Hydrol. Process., 30(15), 2734–2736, doi:10.1002/hyp.10880, 2016.

435   Berghuijs, W. R., Sivapalan, M., Woods, R. A. and Savenije, H. H. G.: Patterns of similarity of seasonal water
436   balances: A window into streamflow variability over a range of time scales, Water Resour. Res., 50(7), 5638–
437   5661, doi:10.1002/2014WR015692, 2014.

438   Blöschl, G., Hall, J., Viglione, A., Perdigão, R. A. P., Parajka, J., Merz, B., Lun, D., Arheimer, B., Aronica, G.
439   T., Bilibashi, A., Boháč, M., Bonacci, O., Borga, M., Čanjevac, I., Castellarin, A., Chirico, G. B., Claps, P.,
440   Frolova, N., Ganora, D., Gorbachova, L., Gül, A., Hannaford, J., Harrigan, S., Kireeva, M., Kiss, A., Kjeldsen, T.
441   R., Kohnová, S., Koskela, J. J., Ledvinka, O., Macdonald, N., Mavrova-Guirguinova, M., Mediero, L., Merz, R.,
442   Molnar, P., Montanari, A., Murphy, C., Osuch, M., Ovcharuk, V., Radevski, I., Salinas, J. L., Sauquet, E., Šraj,
443   M., Szolgay, J., Volpi, E., Wilson, D., Zaimi, K. and Živković, N.: Changing climate both increases and decreases
444   European river floods, Nature, 573(7772), 108–111, doi:10.1038/s41586-019-1495-6, 2019.

445   Clark, M. P., McMillan, H. K., Collins, D. B. G., Kavetski, D. and Woods, R. A.: Hydrological field data from a
446   modeller's perspective: Part 2: Process-based evaluation of model hypotheses, Hydrol. Process., 25(4), 523–543,
447   doi:10.1002/hyp.7902, 2011.

448   Coxon, G., Freer, J., Wagener, T., Odoni, N. A. and Clark, M.: Diagnostic evaluation of multiple hypotheses of
449   hydrological behaviour in a limits-of-acceptability framework for 24 UK catchments, Hydrol. Process., 28(25),
450   6135–6150, doi:10.1002/hyp.10096, 2014.

451   Coxon, G., Addor, N., Bloomfield, J. P., Freer, J., Fry, M., Hannaford, J., Howden, N. J. K., Lane, R., Lewis, M.,
452   Robinson, E. L., Wagener, T. and Woods, R.: CAMELS-GB: hydrometeorological time series and landscape
453   attributes for 671 catchments in Great Britain, Earth Syst. Sci. Data, 12(4), 2459–2483, doi:10.5194/essd-12-
454   2459-2020, 2020.

455   Do, H. X., Gudmundsson, L., Leonard, M. and Westra, S.: The Global Streamflow Indices and Metadata Archive
456   (GSIM) – Part 1: The production of a daily streamflow archive and metadata, Earth Syst. Sci. Data, 10(2), 765–
457   785, doi:10.5194/essd-10-765-2018, 2018.

458   Duan, Q., Schaake, J., Andréassian, V., Franks, S., Goteti, G., Gupta, H. V., Gusev, Y. M., Habets, F., Hall, A.,
459   Hay, L., Hogue, T., Huang, M., Leavesley, G., Liang, X., Nasonova, O. N., Noilhan, J., Oudin, L., Sorooshian,
460   S., Wagener, T. and Wood, E. F.: Model Parameter Estimation Experiment (MOPEX): An overview of science
461   strategy and major results from the second and third workshops, J. Hydrol., 320(1–2), 3–17,
462   doi:10.1016/j.jhydrol.2005.07.031, 2006.

463   Ehret, U., Gupta, H. V., Sivapalan, M., Weijs, S. V., Schymanski, S. J., Blöschl, G., Gelfan, A. N., Harman, C.,
464   Kleidon, A., Bogaard, T. A., Wang, D., Wagener, T., Scherer, U., Zehe, E., Bierkens, M. F. P., Di Baldassarre,
465   G., Parajka, J., van Beek, L. P. H., van Griensven, A., Westhoff, M. C. and Winsemius, H. C.: Advancing
466   catchment hydrology to deal with predictions under change, Hydrol. Earth Syst. Sci., 18(2), 649–671,
467   doi:10.5194/hess-18-649-2014, 2014.

468   Ghiggi, G., Humphrey, V., Seneviratne, S. I. and Gudmundsson, L.: GRUN: an observation-based global gridded
469   runoff dataset from 1902 to 2014, Earth Syst. Sci. Data, 11(4), 1655–1674, doi:10.5194/essd-11-1655-2019, 2019.

470   Gudmundsson, L., Do, H. X., Leonard, M. and Westra, S.: The Global Streamflow Indices and Metadata Archive
471   (GSIM) – Part 2: Quality control, time-series indices and homogeneity assessment, Earth Syst. Sci. Data, 10(2),
472   787–804, doi:10.5194/essd-10-787-2018, 2018.

473   Gupta, H. V., Perrin, C., Blöschl, G., Montanari, A., Kumar, R., Clark, M. and Andréassian, V.: Large-sample
474   hydrology: a need to balance depth with breadth, Hydrol. Earth Syst. Sci., 18(2), 463–477, doi:10.5194/hess-18-
475   463-2014, 2014.

476   Jehn, F. U., Bestian, K., Breuer, L., Kraft, P. and Houska, T.: Using hydrological and climatic catchment clusters
477   to explore drivers of catchment behavior, Hydrol. Earth Syst. Sci., 24(3), 1081–1100, doi:10.5194/hess-24-1081-
478   2020, 2020.

479   Koutsoyiannis, D.: Simple stochastic simulation of time irreversible and reversible processes, Hydrol. Sci. J.,
480   doi:10.1080/02626667.2019.1705302, 2020.

481   Kuentz, A., Arheimer, B., Hundecha, Y. and Wagener, T.: Understanding hydrologic variability across Europe
482   through catchment classification, Hydrol. Earth Syst. Sci., 21(6), 2863–2879, doi:10.5194/hess-21-2863-2017,
483   2017.

484   Linke, S., Lehner, B., Ouellet Dallaire, C., Ariwi, J., Grill, G., Anand, M., Beames, P., Burchard-Levine, V.,
485   Maxwell, S., Moidu, H., Tan, F. and Thieme, M.: Global hydro-environmental sub-basin and river reach
486   characteristics at high spatial resolution, Sci. Data, 6(1), 283, doi:10.1038/s41597-019-0300-6, 2019.

487   Mathai and Mujumdar, P. P.: Multisite Daily Streamflow Simulation With Time Irreversibility, Water Resour.
488   Res., 55(11), 9334–9350, doi:10.1029/2019WR025058, 2019.

489   McMillan, H. K.: A review of hydrologic signatures and their applications, WIREs Water, 8(1), 1–23,
490   doi:10.1002/wat2.1499, 2021.

491   McMillan, H. K., Clark, M. P., Bowden, W. B., Duncan, M. and Woods, R. A.: Hydrological field data from a
492   modeller's perspective: Part 1. Diagnostic tests for model structure, Hydrol. Process., 25(4), 511–522,
493   doi:10.1002/hyp.7841, 2011.

494   Newman, A. J., Clark, M. P., Sampson, K., Wood, A., Hay, L. E., Bock, A., Viger, R. J., Blodgett, D., Brekke,
495   L., Arnold, J. R., Hopson, T. and Duan, Q.: Development of a large-sample watershed-scale hydrometeorological
496   data set for the contiguous USA: data set characteristics and assessment of regional variability in hydrologic model
497   performance, Hydrol. Earth Syst. Sci., 19(1), 209–223, doi:10.5194/hess-19-209-2015, 2015.

498   Richter, B. D., Baumgartner, J. V., Powell, J. and Braun, D. P.: A Method for Assessing Hydrologic Alteration
499   within Ecosystems, Conserv. Biol., 10(4), 1163–1174, doi:10.1046/j.1523-1739.1996.10041163.x, 1996.

500   Sawicz, K., Wagener, T., Sivapalan, M., Troch, P. A. and Carrillo, G.: Catchment classification : empirical
501   analysis of hydrologic similarity based on catchment function in the eastern USA, Hydrol. Earth Syst. Sci., 8(3),
502   2895–2911, doi:10.5194/hess-15-2895-2011, 2011.

503   Sawicz, K. A., Kelleher, C., Wagener, T., Troch, P., Sivapalan, M. and Carrillo, G.: Characterizing hydrologic
504   change through catchment classification, Hydrol. Earth Syst. Sci., 18(1), 273–285, doi:10.5194/hess-18-273-
505   2014, 2014.

506   Serinaldi, F. and Kilsby, C. G.: Irreversibility and complex network behavior of stream flow fluctuations, Phys.
507   A Stat. Mech. its Appl., 450, 585–600, doi:10.1016/j.physa.2016.01.043, 2016.

508   Shamir, E., Imam, B., Morin, E., Gupta, H. V. and Sorooshian, S.: The role of hydrograph indices in parameter
509   estimation of rainfall-runoff models, Hydrol. Process., 19(11), 2187–2207, doi:10.1002/hyp.5676, 2005.

510   Stagge, J. H. and Moglen, G. E.: A nonparametric stochastic method for generating daily climate-adjusted

511   streamflows, Water Resour. Res., 49, 6179–6193, doi:10.1002/wrcr.20448, 2013.

512   Szilagyi, J., Balint, G. and Csik, A.: Hybrid, Markov chain-based model for daily streamflow generation at

513   multiple catchment sites, J. Hydrol. Eng., 11(3), 245–256, 2006.

514

515